Pharm Res (2013) 30:2315–2331
DOI 10.1007/s11095-013-1075-7

RESEARCH PAPER

A Solid-State NMR Study of Amorphous Ezetimibe Dispersions in Mesoporous Silica

Frederick G. Vogt • Karen Roberts-Skilton • Sonya A. Kennedy-Gabb

Received: 24 February 2013 / Accepted: 6 May 2013 / Published online: 22 June 2013

ABSTRACT

Purpose The purpose of this work is to examine the ability of methods based on multinuclear and multidimensional solid-state NMR (SSNMR) to perform detailed characterization of amorphous dispersions of ezetimibe adsorbed on mesoporous silica.

Methods Ezetimibe was loaded into two types of mesoporous silica with average pore sizes of 2.5 and 21 nm. The mesoporous materials were characterized by powder X-ray diffraction (PXRD), vibrational spectroscopy, differential scanning calorimetry, and ^{1}H, ^{13}C, ^{19}F, and ^{29}Si SSNMR analysis including relaxation time measurements. Interactions between the drug and silica were investigated using 1D and 2D SSNMR methods based on dipolar correlation using cross-polarization (CP) and spin diffusion.

Results PXRD was used to show the absence of crystalline ezetimibe in the mesoporous materials, and ^{19}F SSNMR was used to assess drug physical state and study mobility. ^{19}F-^{29}Si CP methods were used to directly detect adsorbed ezetimibe. ^{1}H-^{13}C, ^{1}H-^{19}F, and ^{1}H-^{29}Si, and heteronuclear correlation and ^{1}H homonuclear correlation experiments were used to investigate interactions between the drug and silica through ^{1}H environments.

Conclusions SSNMR methods were able to detect interactions between the drug and the silica substrate. Differences between the drug loaded onto silica with two different pore sizes were observed, including differences in hydrogen bonding environment and molecular mobility. These methods should be useful for characterization of similar systems.

F. G. Vogt • K. Roberts-Skilton • S. A. Kennedy-Gabb
Product Development, GlaxoSmithKline plc., 709 Swedeland Road
King of Prussia, Pennsylvania 19406, USA

Present Address:
F. G. Vogt (✉)
Morgan, Lewis & Bockius, L.L.P., 1701 Market St.
Philadelphia, Pennsylvania 19103-2921, USA
e-mail: fvogt@morganlewis.com

KEY WORDS amorphous dispersion · dipolar correlation · mesoporous silica · powder X-ray diffraction · solid-state NMR

INTRODUCTION

Amorphous phases are increasingly utilized in pharmaceutical development to enhance the dissolution performance of drug molecules with poor aqueous solubility (1,2). Polymers can be used to enhance the stability of amorphous systems by formation of molecular dispersions, in which the potential for crystallization of the drug is greatly reduced while the properties of the amorphous solid are improved (3,4). The stabilization of amorphous drugs can also be accomplished using porous adsorbent media loaded with drug (5). The porous media generally have nanometer-sized pores that constrain crystal growth by preventing the critical nucleation size from being reached, leading to amorphous drug trapped within the nanoporous solid (5). Mesoporous silica is a commonly used material for preparation of such systems because of its high surface area and large pore volume (5). The high surface area leads to a high surface free energy, promoting adsorption of drug molecules on the surface and allowing the system to reach a lower free energy state (5). Improvements in dissolution rate arise from the amorphous nature of the drug and the high surface area of the porous media (5). Drugs may be loaded into mesoporous silica and related mesoporous materials such as folded polysilicate sheets by methods such as solvent or supercritical fluid evaporation or multiple solvent wetting ("impregnation") and drying steps (5,6). Direct sublimation and adsorption of crystals into silica in physical mixtures has also been observed (7,8). Because of the increasing interest in mesoporous silica drug delivery, there is motivation to develop new analytical approaches applicable to the study of these materials, particularly methods that can directly probe the interface between the drug and the silica substrate.

The analytical techniques typically used to probe mesoporous drug delivery systems include differential scanning calorimetry (DSC) and modulated temperature DSC (MDSC) to characterize glass transition temperatures (T_g), powder X-ray diffraction (PXRD) to show the absence of crystalline content, chromatographic or spectroscopic assays to determine drug loading, and techniques to study surface area and porosity (5). Solid-state NMR (SSNMR) is another technique that has been applied to a limited extent in the study of drugs confined in mesoporous materials (9–11). Because amorphous solids confined in nanometer-sized pores can show different molecular dynamics, ^{13}C SSNMR relaxation measurements have been employed to characterize these materials (11). For example, a recent ^{13}C relaxation study showed mobility differences between amorphous indomethacin trapped in a folded-sheet mesoporous material and bulk amorphous indomethacin (12). However, the use of SSNMR in structural studies of drugs adsorbed to mesoporous solids, in which the focus is upon interactions within the amorphous drug or between the drug and the substrate, have been limited. SSNMR has been used extensively to study other types of non-pharmaceutical guest molecules confined within mesoporous silica and related materials (13).

The present work is directed towards using a selection of SSNMR techniques to probe detailed structural aspects of a mesoporous silica drug delivery system. Recently, spectroscopic techniques using two-dimensional (2D) solid-state nuclear magnetic resonance (SSNMR) were shown to readily discriminate between the formation of an amorphous molecular dispersion and the presence of a phase-separated mixture (14,15). These techniques are based the NMR phenomenon of dipolar coupling, which occurs over a short distance range of several Å, and offer an alternative method to assess intermolecular association in cases where existing approaches are not amendable. The SSNMR approaches used for amorphous dispersions were recently extended to the detection of nanometer-scale interactions in a nanocrystalline drug-polymer dispersion (16). The present study uses SSNMR to detect dipolar coupling between a drug and mesoporous silica and directly probe adsorption and molecular association in these systems. Ezetimibe, a fluorinated drug, was chosen as the model system to exploit the utility of ^{19}F SSNMR techniques. Ezetimibe is marketed as a treatment for elevated low-density lipoprotein cholesterol and is currently the subject of clinical trials for safety and efficacy (17). The structure of ezetimibe and the atomic numbering scheme used in this work are shown in Fig. 1. Because of the poor aqueous solubility of ezetimibe, efforts have been made to improve exposure through use of nanocrystalline and stable amorphous forms (18,19). Formulations of ezetimibe adsorbed to mesoporous silica were recently shown to yield enhanced oral exposure in an animal model (19). In the present study, ezetimibe loaded onto two types of mesoporous silica is probed using physical characterization techniques including ^{19}F SSNMR. Molecular mobility of ezetimibe in the two types of silica is explored using relaxation measurements. SSNMR techniques capable of directly detecting ezetimibe adsorption onto silica are demonstrated, including ^{19}F-^{29}Si cross-polarization, ^{1}H 2D spin diffusion, and ^{1}H-^{13}C, ^{1}H-^{19}F, and ^{1}H-^{29}Si heteronuclear correlation experiments. The results are interpreted to show structural and mobility differences between ezetimibe loaded onto two types of mesoporous silica and also to assess the performance of the SSNMR techniques in this type of analysis.

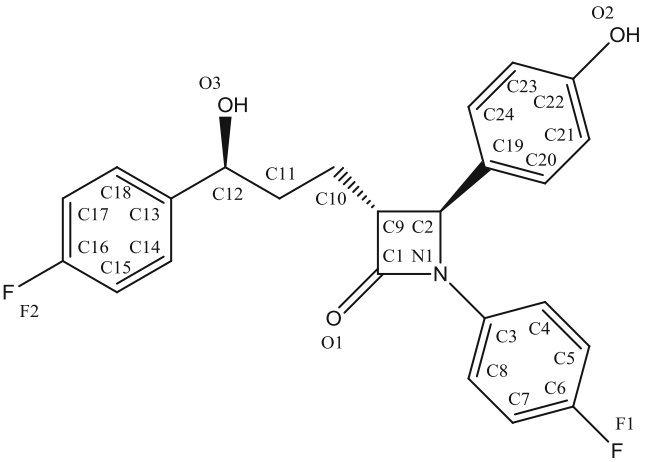

Fig. 1 Chemical structure and atomic numbering scheme of ezetimibe.

MATERIALS AND METHODS

Preparation of Materials

Two grades of mesoporous silica, Sylysia® 350 (SY350) and 740 (SY740), were used in this study (Fuji Silysia Chemical Ltd., Research Triangle Park, NC, USA). The batch of SY350 silica was reported to have a pore volume of 1.6 mL/g, an average pore size of 21 nm, and an average particle size of 3.9 μm. The batch of SY740 silica was reported to have a pore volume of 0.4 mL/g, an average pore size of 2.5 nm, and an average particle size of 5.0 μm. Ezetimibe (AK Scientific, Mountain View, CA, USA) was loaded onto the mesoporous silica using the following procedure. A stock solution of 10 mg ezetimibe delivered as the monohydrate in 100 μL acetone was prepared. This solution was diluted in acetone at volume ratios of 1:20, 1:10, and 1:5 and each resulting solution was added to 200 mg of solid SY350 or SY740 silica. The mixtures were allowed to soak overnight, the remaining liquid was decanted off, and the solids were dried under vacuum at 40°C for 1 week. The different samples prepared with SY350 silica are referred to

here as "ezetimibe-SY350" dispersions, while those prepared with SY740 silica are referred to as "ezetimibe-SY740" dispersions. Amorphous ezetimibe was prepared by melting ezetimibe monohydrate at approximately 180°C and quenching in liquid nitrogen.

PXRD Analysis

X-ray diffraction patterns were obtained using reflection geometry on an X'Pert Pro diffractometer equipped with a real-time multistrip X'Celerator detector (Panalytical, Eindhoven, The Netherlands). The samples were flattened onto zero-background silicon holders and analyzed at ambient temperature and humidity. Samples were scanned in continuous mode from 2 to 40°θ (with a 2θ step size of 0.0167°). CuKα radiation (1.54 Å) was used with a generator power and current of 40 kV and 40 mA, respectively. The sample was rotated with a 1 s revolution time. The incident beam path was equipped with a 0.02 radian Soller slit, a 10 mm beam mask, a 0.5° fixed anti-scatter slit, and a 10 mm programmable divergence slit. The diffracted beam path was equipped with a 10 mm programmable anti-scatter slit, a 0.02 radian Soller slit, and a 0.02 mm nickel filter. Each diffraction pattern required approximately 10 min to acquire. To confirm the identity of the input drug phase, Pawley refinement (20) of the experimental PXRD pattern for crystalline ezetimibe monohydrate was performed using the Reflex module within the Materials Studio version 5.0 software package (Accelrys, San Diego, CA, USA). The unit cell from the previously reported crystal structure of ezetimibe monohydrate was used as input for the Pawley refinement (21). The Pawley fit of the crystalline input material included a polynomial background correction, pseudo-Voigt peak shape profiles, a Bragg-Brentano line shift correction, and Berar-Baldinozzi lineshape asymmetry correction (22,23).

DSC Analysis

DSC and MDSC experiments were performed using a Q2000 instrument (TA Instruments, Inc., New Castle, DE, USA). Samples with masses of 3 to 5 mg were heated in closed aluminum pans with lids that were not crimped. Nitrogen was used as purge gas with a flow rate of 20 mL/min. For DSC analyses, two heating rates of 10°C/min and 0.5°C/min were employed over a temperature range of 25 to 250°C. For MDSC experiments, samples were heated from 0 to 250°C at 2°C/min using an amplitude of ±0.32°C and a modulation period of 60 s. An experiment on crystalline ezetimibe monohydrate was carried out in quench-cool mode, where the sample was heated to 180°C, cooled to 0°C, and then heated again to 300°C to observe the glass transition. This method was chosen based on prior DSC experiments that established the peak temperature of the melting endotherm of crystalline ezetimibe monohydrate as 162°C. Data analysis was performed using the Universal Analysis 2000 software (TA Instruments, New Castle, DE, USA). The instrument was calibrated using a sample of sapphire for heat capacity and a sample of indium for enthalpy and temperature.

Infrared and Raman Spectroscopy

IR spectra were obtained using a Perkin-Elmer Spectrum One Fourier transform IR spectrometer equipped with a DTGS (deuterated triglycine sulfate) detector (Perkin-Elmer, Waltham, MA, USA). A total of 16 scans were averaged at a resolution of 2 cm^{-1} for each of the spectra, requiring approximately 10 min per spectrum. Spectra were obtained using a single-bounce attenuated total reflectance (ATR) accessory with a diamond window. Samples were covered with a glass slide and pressed against the window for analysis. Raman spectra were obtained using a Bruker MultiRAM Fourier transform Raman spectrometer using a resolution of 2 cm^{-1} with collection of the 180° scattered signal (Bruker Optics, Billerica, MA, USA). The system is equipped with a long-hold nitrogen-cooled germanium diode detector (Bruker Optics, Billerica, MA, USA). Laser excitation was performed using a 1 W, 1.064 μm diode-pumped neodymium-doped yttrium aluminum garnet (Nd:YAG) laser that was attenuated to 0.5 W for the analyses presented here (Klastech GmbH, Dortmund, Germany). Samples were placed in 5 mm outer diameter borosilicate glass tubes for analysis, and 512 scans were acquired.

UV-Visible Spectroscopy

Solution-phase UV-visible spectra were recorded using a Varian Cary 50 spectrometer (Agilent, Palo Alto, CA, USA). Solutions were prepared using spectroscopic grade acetonitrile and were scanned from 200 to 700 nm at a scan rate of 50 nm/min to obtain the spectral properties of ezetimibe. For quantitative measurements, calibration was performed at three concentrations using an observation wavelength of 231 nm (corresponding to the wavelength with maximum absorbance for ezetimibe). A slit width of 1.5 nm and an integration time of 1 s were used. The mesoporous solids were sonicated overnight to release drug into acetonitrile prior to quantitative analysis to determine the quantity of drug present.

Surface Area Measurements

Specific surface area was measured using a Tristar 3000 instrument (Micromeritics, Norcross, GA, USA). Nitrogen

was used as the adsorbate in the experiments. The surface area was calculated using a seventeen-point Brunauer-Emmett-Teller (BET) model.

SSNMR Analysis

SSNMR experiments were performed using three NMR instruments, an Avance spectrometer with a static field of 9.4 T, an Avance II+ spectrometer with a static field of 11.7 T, and an Avance III spectrometer with a static field of 16.4 T (Bruker Biospin, Inc., Billerica, MA, USA). These spectrometers operate at ^{1}H frequencies of 399.87, 500.08, and 700.13 MHz, respectively. ^{13}C, ^{29}Si, and ^{19}F SSNMR spectra were obtained at 9.4 T and 11.7 T using a Bruker 4 mm magic-angle spinning (MAS) probe triply-tuned to ^{1}H, ^{19}F, and X-nucleus frequencies (where the X-nucleus was either ^{13}C or ^{29}Si). Cross-polarization (CP) transfers were performed at radiofrequency power levels of 40 to 80 kHz. The power level was ramped linearly downward during the contact time on the ^{1}H channel to enhance CP efficiency (24). ^{19}F CP-MAS spectra were obtained at an MAS rate (ν_r) of 12.5 kHz using a 10 s relaxation delay. ^{13}C CP spectra were obtained with ν_r set to 8 kHz unless otherwise noted and were recorded using a five-pulse total sideband suppression (CP-TOSS) sequence with a 10 s relaxation delay (25). Edited ^{13}C CP-TOSS spectra containing only quaternary and methyl signals were obtained using dipolar dephasing (also known as non-quaternary suppression or NQS) during the TOSS period and three subsequent rotor periods using a shifted echo pulse sequence (25,26). ^{29}Si spectra were obtained using both DP-MAS and CP-MAS sequences. ^{1}H heteronuclear decoupling for ^{13}C, ^{19}F, and ^{29}Si experiments was performed at a radiofrequency (RF) power of 105 kHz using the SPINAL-64 pulse sequence (27). ^{19}F-^{29}Si CP-MAS experiments were performed using a ramp on the ^{19}F channel similar to that used for experiments that used ^{1}H as the CP source. A sample of sodium hexafluorosilicate (Sigma-Aldrich, St. Louis, MO, USA) was used to optimize ^{19}F-^{29}Si CP conditions (28). ^{1}H spectra were obtained at several fields using direct polarization at high MAS rates (referred to here as the DP-MAS experiment) using a single excitation pulse without decoupling during acquisition, and were also obtained at 16.4 T using the windowed DUMBO homonuclear decoupling sequence during acquisition (29).

Reference materials were obtained from Sigma-Aldrich (St. Louis, MO, USA). ^{13}C spectra were referenced to tetramethylsilane (TMS) using hexamethylbenzene as an external standard *via* the methyl resonance at 17.36 ppm (30). ^{19}F spectra were referenced to $CFCl_3$ by the unified scale method (31), and further checked against an external standard of flurbiprofen with a reported shift of −115.0 ppm (32). ^{29}Si spectra were referenced against TMS using an external standard of tetrakis(trimethylsilyl)silane as the secondary reference, using the more intense deshielded peak at −9.86 ppm for referencing (33). ^{1}H spectra were referenced externally to a sample of crystalline L-alanine, with the methyl resonance set to 1.6 ppm; this value was determined by addition of a small amount of liquid TMS to the rotor containing L-alanine.

Proton spin–lattice relaxation times (^{1}H T_1) were determined *via* ^{19}F- and ^{29}Si-detected saturation recovery experiments using CP using non-linear fitting of 16 time points. A 100-pulse saturation comb was used to suppress ^{1}H magnetization. ^{19}F spin–lattice relaxation times (^{19}F T_1) were determined using a pulse sequence with CP enhancement by non-linear fitting of 16 points (34). ^{19}F spin–lattice relaxation times in the rotating frame (^{19}F $T_{1\rho}$) were determined using an additional variable ^{19}F spin-lock pulse after CP by non-linear fitting of eight time points (35). During the ^{19}F variable pulse period of the ^{19}F $T_{1\rho}$ measurement, the ^{1}H RF power was turned off to prevent drain *via* CP. Relaxation data was fitted using the Topspin software package, version 1.3 (Bruker Biospin, Inc., Billerica, MA, USA). Where noted, relaxation times were measured as five replicate experiments, and the average is reported along with a 99.7% confidence interval (CI), which was calculated as ± three times the standard deviation.

2D CP heteronuclear correlation (CP-HETCOR) experiments between ^{1}H and ^{13}C, ^{19}F, and ^{29}Si nuclei were obtained at 11.7 T using a 4 mm HFX probe with ν_r set to 14 kHz and frequency-switched Lee-Goldburg (FSLG) homonuclear decoupling at 105 kHz (36). The HETCOR experiments were performed so that the entire spectrum was recorded with $F_1 > 0$ Hz, where F_1 is the indirectly-detected ^{1}H frequency dimension and F_2 is the directly-detected dimension. This approach avoids interference from quadrature images and artifacts in the ^{1}H spectrum at $F_1 = 0$ Hz that occur with the CP-HETCOR experiment.

Computational Methods

^{19}F chemical shielding calculations were performed using a molecular cluster extracted from the crystal structure of ezetimibe monohydrate (21), after hydrogen positions were optimized using a density functional theory (DFT) calculation with periodic boundary conditions using the DMol3 package in Materials Studio version 5 (Accelrys, San Diego, CA, USA) (37,38). The HCTH/407 generalized gradient approximation (GGA) density functional (also known as the HCTH functional) was used with a double numerical basis set with polarization functions on all atoms (the DNP basis set) (37–40). A 2×1×1 **k**-point set was used for the hydrogen geometry optimization calculation. From the optimized periodic structure, a cluster consisting of six ezetimibe molecules was selected that was chosen to provide nearest-

neighbor surroundings for both fluorine sites. The Gaussian 09W package (Gaussian, Inc., Wallingford, CT, USA) was used for gauge-including atomic orbital (GIAO) NMR shielding calculations on the cluster (41). The B3LYP hybrid density functional was used for the GIAO NMR calculations (42). A locally-dense basis set was employed using the 6-311+G(2d,p) basis set for the two central fluorine positions and the 3-21G basis set for all other atoms (including other fluorine atoms) in the molecular cluster (43).

RESULTS AND DISCUSSION

Initial Characterization

Initial solid-state characterization of the mesoporous silica materials loaded with ezetimibe was performed using PXRD, DSC, and ^{19}F SSNMR spectroscopy. First, the identity of the crystalline input material was determined using PXRD. The PXRD pattern of crystalline input ezetimibe was found to match that predicted from the single crystal structure reported for a monohydrate phase of this compound after Pawley refinement, as shown in Fig. 2a (20,21). A weighted-profile residual value (R_{wp}) of 10.15% and a non-weighted residual value (R_p) of 7.10% were obtained from the Pawley refinement (22).

The PXRD patterns of the mesoporous silica samples loaded with ezetimibe are shown in Fig. 2b. The drug content for each sample determined by quantitative UV-visible spectroscopy is also shown in Fig. 2b. The patterns show no evidence of reflections that would indicate the presence of crystalline components. Only a broad diffusive scattering pattern caused by amorphous material is observed in all three concentrations of drug in both SY350 and SY740 silica. The PXRD patterns for the ezetimibe-SY350 dispersions exhibit diffuse scattering maxima in the vicinity of about 22 °2θ. The patterns for the ezetimibe-SY740 dispersions show maxima that are shifted to approximately 23 °2θ, which corresponds to a smaller *d*-spacing and is consistent with the smaller pore size within this grade of silica. For comparison, the PXRD pattern of amorphous ezetimibe prepared by the melt-quench procedure is also shown in Fig. 2b. The maximum of the diffuse scattering in amorphous ezetimibe appears at about 20 °2θ and differs from the patterns obtained from the ezetimibe dispersions in SY350 and SY740.

The presence of fluorine atoms in the structure of ezetimibe allows for the use of the sensitive and specific ^{19}F nucleus for an initial SSNMR assessment of the ezetimibe-SY740 and ezetimibe-SY740 dispersions. Figure 3 shows the ^{19}F CP-MAS spectra of the six batches prepared for this study in comparison to input ezetimibe monohydrate and amorphous ezetimibe. The two fluorine resonances in crystalline ezetimibe are assigned as shown in Fig. 3 based on the GIAO DFT calculation of ^{19}F chemical shielding using a molecular cluster taken from the reported ezetimibe monohydrate crystal structure after hydrogen geometry optimization (21). The F1 position was calculated to have an absolute chemical shielding of 313.7 ppm, which is about 18 ppm more shielded than the calculated absolute

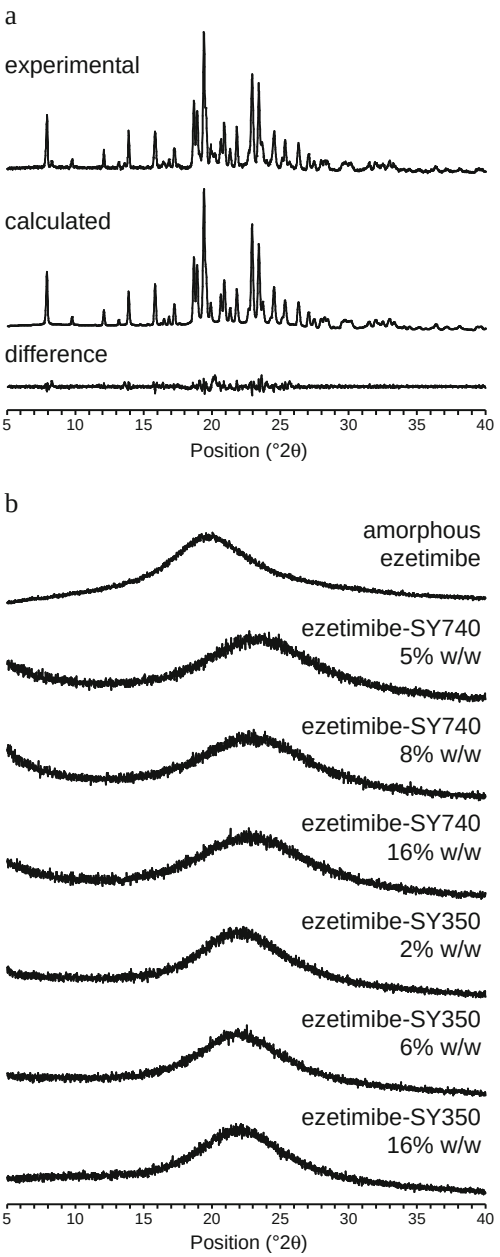

Fig. 2 (**a**) Reflection PXRD patterns of the crystalline ezetimibe monohydrate used as input in this study, compared to a Pawley fit against a reported monohydrate crystal structure (see text). (**b**) Reflection PXRD patterns of the mesoporous silica materials loaded with ezetimibe used in this study and amorphous ezetimibe made by the melt-quench procedure. The drug loading (in % w/w) determined by UV-visible spectroscopy is shown for each of the mesoporous silica samples.

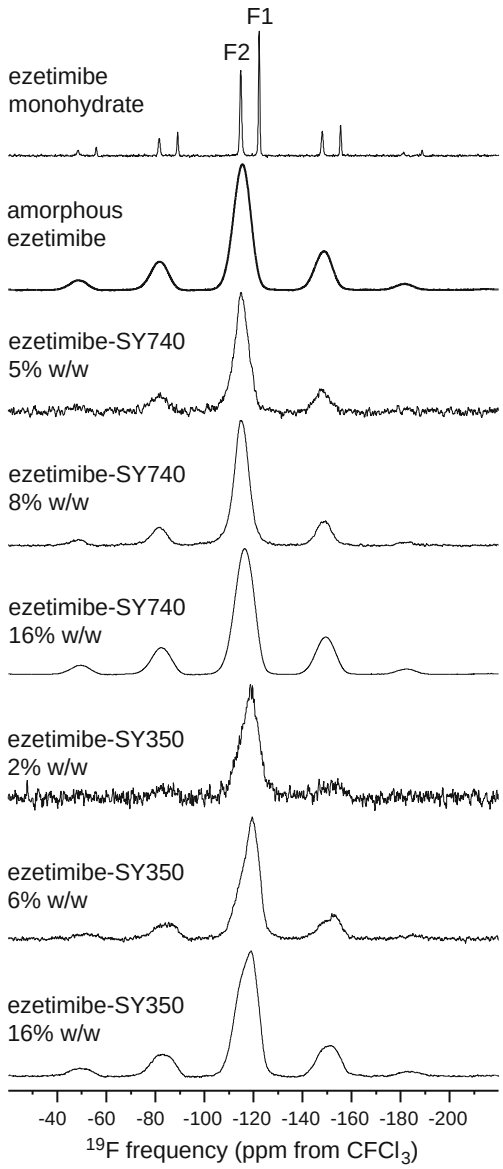

Fig. 3 ^{19}F CP-MAS spectra ($\nu_r = 12.5$ kHz) of crystalline ezetimibe monohydrate, amorphous ezetimibe, and the mesoporous silica materials loaded with ezetimibe used in this study. The assignments shown refer to the numbering scheme given in the text. Each of the spectra of the dispersions was obtained using 8,192 scans requiring 12 h of acquisition time. The spectra of ezetimibe monohydrate and amorphous ezetimibe were recorded using 128 scans. Spectra were obtained at 9.4 T and 273 K. The drug loading (in % w/w) determined by UV-visible spectroscopy is shown for the mesoporous silica samples.

shielding for the F2 position of 295.9 ppm. As a result, F1 is assigned to the more shielded fluorine resonance observed for ezetimibe monohydrate in Fig. 3 with a chemical shift of −122.3 ppm, and F2 is assigned to the resonance at −114.8 ppm. These two fluorine positions are not clearly resolved in the broadened lineshapes observed for the drug-loaded mesoporous silica samples in Fig. 3, although the SY350 dispersions show evidence of increased intensity towards the more shielded side of the ^{19}F signals that could be indicative of a change in fluorine environment (perhaps involving F1) in comparison to the SY740 dispersions.

The spectra of the dispersions in Fig. 3 were each obtained using 8,192 scans and a 10 s relaxation delay, which required approximately 12 h. An increased number of scans and a longer-than-necessary relaxation delay were used to allow for detection of any crystalline material, if present. No crystalline material is detected in the ^{19}F spectra of the dispersions, providing a sensitive means to exclude crystalline content even with low drug levels. The variability in the signal-to-noise of the ^{19}F CP-MAS spectra in Fig. 3 is caused by the differences in drug load. All of the spectra were obtained using the same conditions, so that the magnitude of the ^{19}F CP-MAS spectrum for each sample correlates with the drug content determined by UV-visible spectroscopy. For example, at the lowest drug concentration, the SY740 silica showed slightly higher drug loadings by UV-visible spectroscopy, which is reflected in the ^{19}F spectra. Finally, the ^{19}F spectra obtained from the ezetimibe-SY350 dispersions show more intensity in the shielded region of the broad centerband lineshape in comparison to the spectra obtained from the ezetimibe-SY740 dispersions, which show a more symmetric lineshape. This suggests a possible structural difference between the amorphous phases loaded on each type of silica.

Vibrational Spectroscopy and Thermal Analysis

Based on the PXRD and ^{19}F SSNMR results, which showed no detectable difference within each set of three samples besides ezetimibe concentration, more detailed structural analysis was progressed using the highest drug content dispersions (16% w/w) prepared from both the SY740 and SY350 silica. Expanded regions of IR spectra of these two batches obtained using ATR sampling are shown in Fig. 4, where they are compared to the spectra of the input materials. Strong absorbance bands from the silica are observed in the region between 1,250 and 650 cm^{-1}. Both input silica materials show a band at 1,632 cm^{-1}, annotated in Fig. 4, which is assigned to water bound to silanol groups in the mesoporous structure. Another band assigned to water is observed in both input silica materials at about 3,377 cm^{-1} (not shown). After drug loading, a strong band due to ezetimibe is observed at 1,511 cm^{-1} in both dispersions, which is slightly shifted from its position of 1,507 cm^{-1} in crystalline ezetimibe.

The frequency of the carbonyl band at approximately 1,720 cm^{-1} (assigned to the C1-O1 stretching vibration) can be related to hydrogen bonding differences in the dispersions. Shifts in carbonyl band positions occur as a result of the interaction of the lone pairs on the oxygen with a hydrogen donor group, which increases the electronic

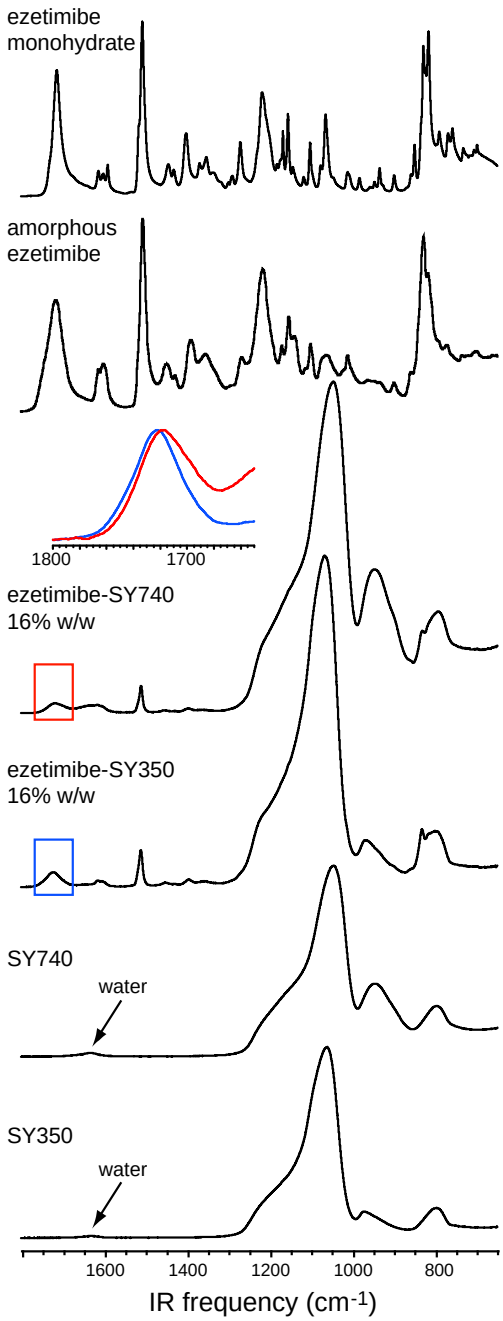

Fig. 4 Comparison of ATR IR spectra of crystalline ezetimibe monohydrate, amorphous ezetimibe, both input silica phases, and two mesoporous silica dispersions with ezetimibe used in this study with 16% w/w drug loading. The *inset* highlights changes in the carbonyl band (*boxed regions*) for ezetimibe-SY740 (*red*) and ezetimibe-SY350 (*blue*).

polarization of the double bond. This in turn causes weakening of the carbonyl bond, which shifts the frequency of the carbonyl stretch to lower wavenumbers (44,45). The shift to lower wavenumbers increases as the oxygen accepts shorter hydrogen bonds. In the crystal structure of ezetimibe monohydrate, the carbonyl group accepts a hydrogen bond from a molecule of water of hydration, and consequently this band appears with a maximum of 1,714 cm^{-1} in crystalline ezetimibe. The amorphous ezetimibe produced by the melt-quench procedure exhibits a band at 1,716 cm^{-1}, indicative of longer hydrogen bonds to the O1 acceptor. The carbonyl band is observed at 1,722 cm^{-1} in the ezetimibe-SY350 dispersion and at 1,718 cm^{-1} in the ezetimibe-SY740 dispersion. The ezetimibe-SY740 dispersion shows evidence of shorter hydrogen bonds to the O1 acceptor than the ezetimibe-SY350 dispersion. These hydrogen bonds could be intermolecular or could involve water and/or silica. Both dispersions show reduced hydrogen bonding compared to crystalline and amorphous ezetimibe. This effect provides important structural information, and is discussed in more detail below after consideration of SSNMR results. FT-Raman spectra of the samples (not shown) did not highlight any additional differences in the ezetimibe vibrational bands when loaded onto either SY350 or SY740 that could be interpreted for additional insight into structural differences.

MDSC analysis was also performed on the two dispersions containing 16% w/w of ezetimibe. For the 16% w/w ezetimibe-SY740 dispersion, the MDSC reversing heat flow showed a T_g event at 88°C. A glass transition was not detected for the 16% w/w ezetimibe-SY350 dispersion. The lack of a glass transition detectable by MDSC is not uncommon for mesoporous silica dispersions and has also been observed for a dispersion of itraconazole on mesoporous SBA-15 silica (5,46). A possible explanation for this effect is that the layer of ezetimibe deposited on the SY740 silica is too thin to yield a T_g because of the high surface area of this type of silica. The pre-loaded surface area of the SY740 silica used in this study was determined by BET nitrogen adsorption to be 508 m^2/g, while the SY350 silica was determined to have a lower pre-loaded surface area of 260 m^2/g. The T_g observed for amorphous ezetimibe was 64°C, and was obtained by MDSC after creating amorphous ezetimibe in the pan by heating beyond the melting point of crystalline ezetimibe monohydrate to 180°C, cooling, and reheating in the DSC pan.

Assessment of Differences in Drug Mobility Using ^{19}F Relaxation Times

^{19}F T_1 and $T_{1\rho}$ relaxation measurements were used as a probe of mobility differences in the 16% w/w ezetimibe-SY740 and ezetimibe-SY350 dispersions. Although not previously reported in an application to a mesoporous pharmaceutical dispersion, these experiments can be used in the same manner as with ^{13}C relaxation time measurements. For example, ^{13}C $T_{1\rho}$ analysis was recently employed to demonstrate mobility differences of a drug in two different pore sizes of mesoporous silica (11). ^{19}F T_1 and $T_{1\rho}$ relaxation analysis allows for greater sensitivity when lower amounts of drug are present as with the present materials.

The sensitivity of the ^{19}F nucleus, which has a relative receptivity of that is nearly 5,000 times that of ^{13}C, also offers the possibility of replicate relaxation time measurements with high signal-to-noise in a reasonable time (31). This in turn allows for thorough assessment of both experimental error and potential changes in relaxation time caused by the effects of spinning forces or other potential spinning effects such as the displacement of paramagnetic O_2 gas with N_2 gas in the porous materials.

The ^{19}F $T_{1\rho}$ values of the 16% w/w dispersions were assessed as an indicator of molecular mobility in the kHz frequency range for the amorphous drug (11), with the results summarized in Table I. The ^{19}F $T_{1\rho}$ values were determined using five replicate measurements (with each experiment requiring 3 h) to obtain error estimates. The ^{19}F $T_{1\rho}$ value of the 16% w/w ezetimibe-SY740 dispersion was found to be longer than that of the 16% w/w ezetimibe-SY350 dispersion. The average $T_{1\rho}$ times from the two samples are within about 15% of each other. However, the 99.7% CI ranges obtained from five replicate measurements do not overlap, indicating that the difference in ^{19}F $T_{1\rho}$ times is significant. The shorter $T_{1\rho}$ time for ezetimibe in the larger pore size SY350 silica is indicative of greater molecular mobility in the kHz frequency range of the drug in this material. These results are consistent with a recent study that compared ^{13}C $T_{1\rho}$ values of another drug loaded onto SY740 and SY350 silica, which observed a similar trend (11). In comparison, the $T_{1\rho}$ value measured for amorphous ezetimibe produced by melt-quench was intermediate between the two dispersions and is indicative of the same general degree of molecular mobility in the kHz frequency range amongst all three amorphous materials.

The ^{19}F T_1 values of the 16% w/w dispersions are also reported in Table I. The ^{19}F T_1 value of the 16% w/w ezetimibe-SY350 dispersion was observed to increase as temperature was reduced. This observation is consistent with the ^{19}F nuclei in the ezetimibe-SY350 dispersion being in the slow motional regime with respect to the Larmor frequency. This trend agreed with that observed for amorphous ezetimibe produced by the melt-quench procedure, where the ^{19}F T_1 value also increased at a lower temperature. However, the opposite trend was observed for the ezetimibe-SY740 dispersion, which also exhibited much shorter overall ^{19}F T_1 values. The observation that relaxation times obtained at higher temperatures were longer than at low temperatures indicates that the drug in the smaller pore size SY740 silica sits in the fast motional regime with respect to the Larmor frequency. The ^{19}F T_1 results for the ezetimibe-SY740 dispersion suggests faster aromatic ring motion in the smaller pore size material, perhaps because more drug surface area is exposed, allowing fluoroaryl groups to move more rapidly at the surface. The high level of residual acetone trapped in the ezetimibe-SY740 dispersion (see below) is a likely cause of the short relaxation times and faster motion observed in this material.

^{13}C and ^{29}Si SSNMR Characterization

More detailed structural information can be gained using SSNMR analysis of two important nuclei in this system, the ^{13}C and ^{29}Si nuclides, both of which offer high resolution spectra but are considerably less sensitive that the ^{19}F nucleus. ^{13}C CP-TOSS spectra of the 16% w/w ezetimibe-SY740 and ezetimibe-SY350 dispersions are shown in Fig. 5. The ^{13}C spectral assignments given in Fig. 5 refer to the numbering scheme shown for ezetimibe in Fig. 1. A number of ^{13}C resonances can be assigned as shown in Fig. 5 for crystalline ezetimibe monohydrate based on established ^{13}C chemical shift trends although the aromatic region is highly overlapped (47). In the dispersions, spectral overlap in the region between 138 and 110 ppm prevents assignments of specific resonances to the C4, C5, C7, C8, C14, C15, C17, C18, C20, C21, C23, and C24 positions, which are labeled "aromatics" in Fig. 5. The addition of ^{19}F decoupling to the ^{1}H decoupling used in the ^{13}C CP-TOSS experiments did not offer any improvement in the resolution of the amorphous ezetimibe because of the significant broadening caused by the range of chemical shift environments in these amorphous materials (14).

Despite the overall similarity of the spectra, ^{13}C CP-TOSS experiments show the peak assigned to C1 to be more deshielded in the ezetimibe-SY740 dispersion than for the ezetimibe-SY350 dispersion. This peak has a maximum of 170.6 ppm in the ezetimibe-SY350 dispersion, which shifts to 171.0 ppm in the ezetimibe-SY740 dispersion. The ezetimibe-SY740 dispersion thus shows evidence

Table I Summary of Relaxation Time Measurements for the Mesoporous Silica Materials Loaded with Ezetimibe Used in this Study and the Amorphous Ezetimibe Produced by the Melt-Quench Process. All Measurements were Performed at 9.4 T with v_r set to 12.5 kHz. Error was Calculated as a 99.7% CI as Described in the Text from Five Replicate Measurements

Relaxation time	Measurement temperature (K)	16% w/w ezetimibe-SY740	16% w/w ezetimibe-SY350	Amorphous ezetimibe
^{19}F $T_{1\rho}$	298	4.81 ± 0.08 ms	4.27 ± 0.27 ms	4.43 ± 0.10 ms
^{19}F T_1	298	0.94 ± 0.02 s	3.17 ± 0.13 s	5.98 ± 0.08 s
^{19}F T_1	273	0.78 ± 0.02 s	4.43 ± 0.16 s	8.46 ± 0.17 s

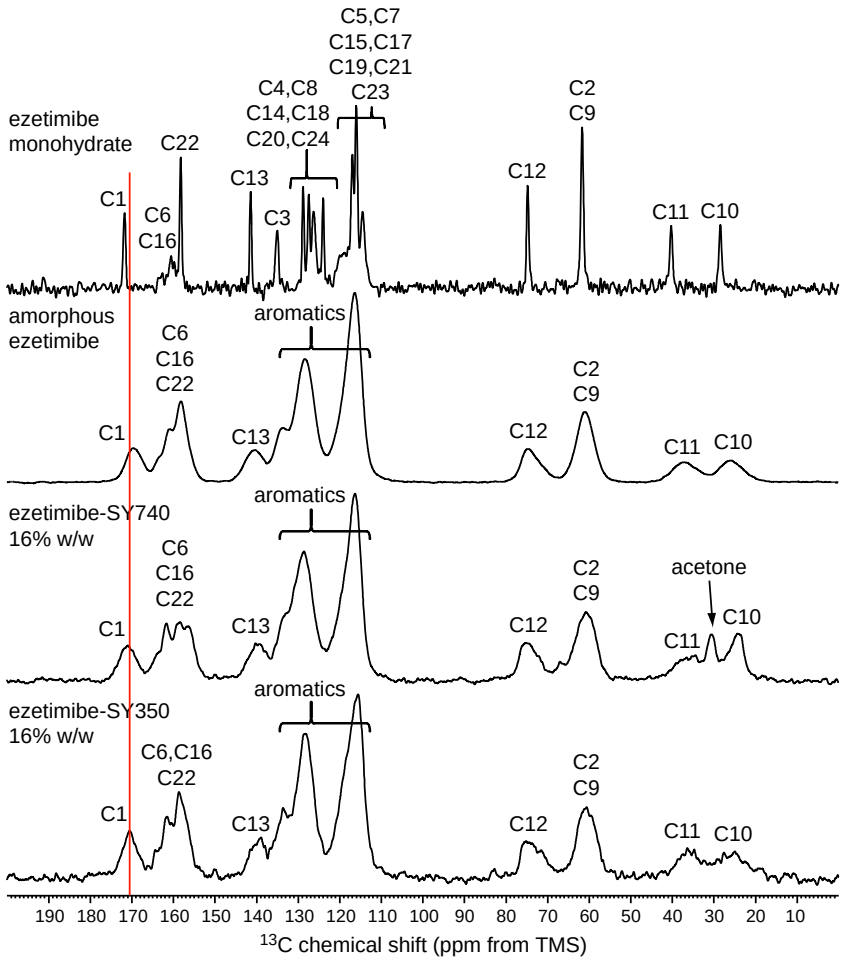

Fig. 5 ^{13}C CP-TOSS spectra ($\nu_r = 8$ kHz) of crystalline ezetimibe monohydrate, amorphous ezetimibe, and two mesoporous silica materials loaded with 16% w/w ezetimibe. The assignments shown refer to the numbering scheme given in Fig. 1. A peak assigned to residual acetone is noted on the spectrum of ezebimite loaded onto SY740 mesoporous silica. The *red line* is a guide to the eye to highlight shift changes in the C1 resonance discussed in the text. Spectra were obtained at 9.4 T and 273 K.

of shorter hydrogen bonding to O1, as more deshielded ^{13}C carbonyl shifts occur with shorter hydrogen bonds (48). This ^{13}C chemical shift trend for the dispersions is consistent with the trend in IR frequency for the carbonyl band. Crystalline ezetimibe exhibits a ^{13}C shift for C1 of 171.8 ppm, again consistent with a hydrogen bond between O1 and the bound water of hydration. In the spectrum of amorphous ezetimibe prepared by the melt-quench procedure, the C1 position shows a shift of 169.8 ppm, consistent with the lengthening or loss of a hydrogen bond to O1. Unlike the IR results, the ^{13}C SSNMR results for the C1 resonance suggest that both dispersions show shorter hydrogen bonds involving O1 than amorphous ezetimibe. Finally, the overall lineshape of the C1 resonance also changes between the dispersions; like the changes seen in the ^{19}F lineshape, this suggests a change in the ezetimibe structural environment between the two types of silica.

A strong signal from bound acetone is visible at approximately 30 ppm in the ^{13}C spectrum of the ezetimibe-SY740 dispersion in Fig. 5, which remained even after extensive drying. The acetone is detected using CP, indicating that it is bound within the solid. The presence of acetone in the amorphous ezetimibe regions adsorbed within the silica may be the cause of greatly increased ezetimibe mobility detected by the relaxation time analysis for this material.

^{29}Si DP-MAS spectra of the mesoporous silica samples loaded with ezetimibe are shown in Fig. 6a. The spectra were obtained with ^{1}H decoupling and required a 60 s relaxation delay. Resonances can be assigned based on established chemical shift trends for ^{29}Si in silica and silicate materials (49). The assignments shown in Fig. 6a make use of Q_n notation, where Q is used to indicate that four oxygens are attached to silicon, and where n is equal to the number of bridging oxygen sites (i.e. Si-O-Si bridges). No monomeric (Q_0) or end-group (Q_1) silicon sites are observed in the spectra. Polymeric groups assigned to Q_2, Q_3, and Q_4 are observed. The ^{29}Si DP-MAS spectra of the 16% w/w ezetimibe-SY350 and ezetimibe-SY740 samples are indistinguishable from the spectra of their respective input silica batches. ^{29}Si CP-MAS spectra of the same samples are shown in Fig. 6a. These spectra support the assignments in Fig. 6a because the sites containing one (Q_3) and two (Q_2) residual silanol groups show increased signal intensity relative to their corresponding DP-MAS spectra. The presence of ezetimibe in the mesoporous silica has little to no discernible effect on either the ^{29}Si DP-MAS or

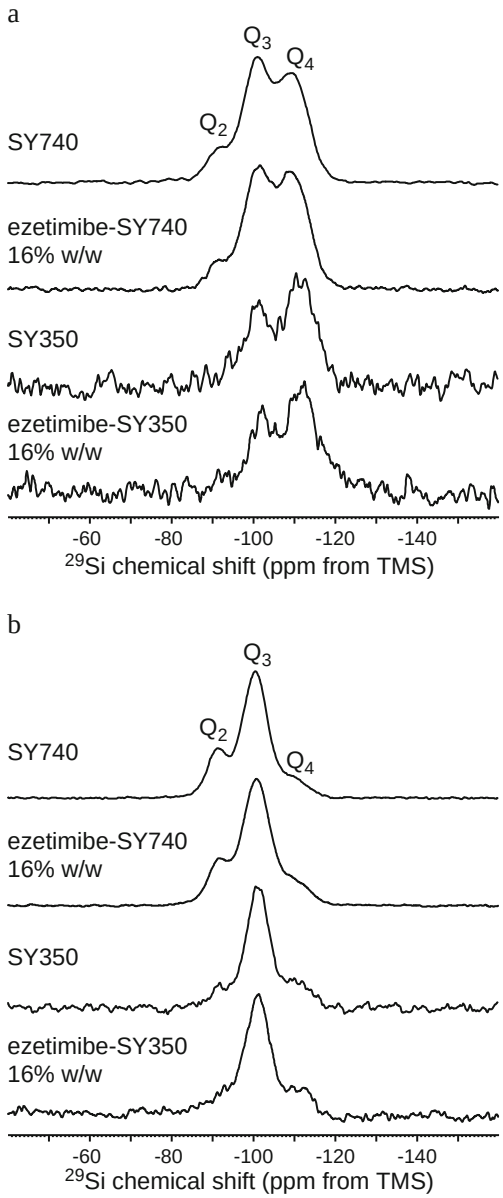

Fig. 6 (**a**) ^{29}Si DP-MAS and (**b**) CP-MAS spectra ($\nu_r = 8$ kHz) of two mesoporous silica materials with the highest ezetimibe loading. The assignments shown refer to the number of bridging oxygen sites (see text). Spectra were obtained at 9.4 T and 273 K.

CP-MAS spectra, suggesting that while these spectra report on the internal structure of silica in mesoporous drug dispersions, other techniques are needed to study the interactions between the drug and the silica.

^{19}F-^{29}Si CP SSNMR Experiments

CP between ^{19}F and ^{29}Si nuclei can potentially be used to selectively observe the interface between ezetimibe and silica. ^{19}F-^{29}Si CP experiments have not been reported in a study of a pharmaceutical mesoporous system although they have been used to successfully characterize other materials (28,50). The results of a 1D ^{19}F-^{29}Si CP experiment using a 5 ms contact time on the ezetimibe dispersion on SY740 are shown in Fig. 7. The ^{19}F-^{29}Si CP spectrum is similar in appearance to the ^{1}H-^{29}Si CP spectrum, indicating that all of the silicon sites (Q_2, Q_3, and Q_4) are able to participate in dipolar coupling with the fluorine positions in ezetimibe, suggesting that the ezetimibe is in close proximity to all three types of silicon site. The spectrum shown in Fig. 7 required 18 h to obtain. No detectable ^{19}F-^{29}Si CP signal was obtained after the same time period for the drug dispersed onto SY350. While very useful when signal is obtained, this result shows that the ^{19}F-^{29}Si CP experiment does not have sufficient sensitivity for low drug content dispersions to be generally applicable without potentially impractical experimental times.

^{1}H SSNMR Experiments

The ^{1}H DP-MAS spectra obtained at 700 MHz for the 16% w/w dispersions of ezetimibe in the two grades of mesoporous silica are shown in Fig. 8a. For comparison, the similarly-obtained ^{1}H DP-MAS spectra of crystalline ezetimibe, amorphous ezetimibe obtained by the melt-quench process, and SY350 and SY740 silica are also shown. Crystalline ezetimibe displays distinct aromatic and aliphatic ^{1}H resonances; the more shielded of the aromatic resonances at about 6 ppm most likely arises from energetically-favorable aromatic π–stacking interactions, which are not observed in amorphous ezetimibe. In the 16% w/w dispersion of ezetimibe in SY740, at least three distinct resonances are resolved in the ^{1}H spectrum in Fig. 8a. Based on the spectra of the input materials, these major ^{1}H resonances are assigned to the aromatic protons in ezetimibe, silanol groups on SY740 interacting with water,

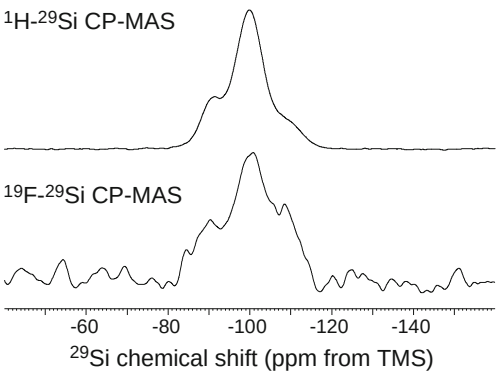

Fig. 7 Comparison of ^{19}F-^{29}Si CP-MAS spectrum of 16% w/w ezetimibe-SY740 dispersion with the conventional ^{1}H-^{29}Si CP-MAS spectrum of the same sample. The ^{19}F-^{29}Si CP-MAS spectrum was obtained with a 5 ms contact time. Both spectra were obtained with $\nu_r = 8$ kHz. A similar experiment performed on the sample containing 16% w/w ezetimibe loaded onto SY350 silica yielded no signal after a similar experimental duration. Spectra were obtained at 11.7 T and 273 K.

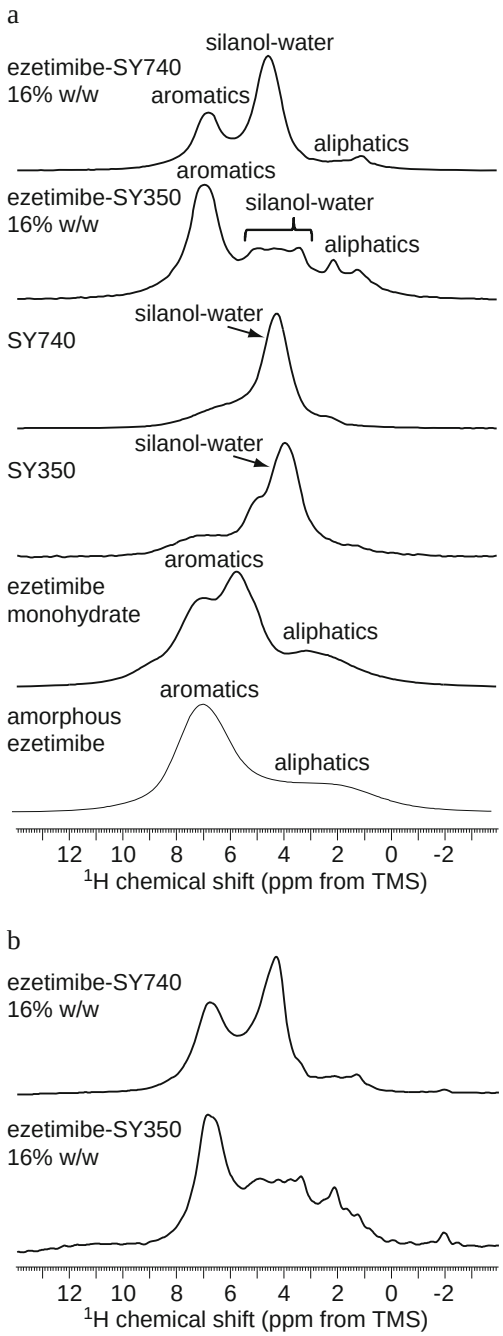

Fig. 8 (**a**) ^{1}H DP-MAS spectra ($\nu_r = 35$ kHz) of the mesoporous silica materials loaded with ezetimibe and input materials used in this study. (**b**) ^{1}H spectra obtained with DUMBO decoupling ($\nu_r = 30$ kHz). Spectra were obtained at 16.4 T and 273 K.

and aliphatic groups in ezetimibe. Residual water in a mesoporous silica material is normally associated with silanol groups as a single, broad resonance, and isolated silanol groups that do not interact with water (typically at <2 ppm) were not observed in the SY740 spectrum (51,52). The use of windowed DUMBO homonuclear decoupling in conjunction with fast MAS to record the ^{1}H spectrum of this material, as shown in Fig. 8b, did not yield any significant improvement in resolution (29). This indicates that the broadening seen in the spectrum is not limited by ^{1}H-^{1}H dipolar coupling but by the amorphous nature of the material. The ^{1}H chemical shifts of acidic silanol groups are known to be sensitive to hydrogen bonding, and the largest peak in the spectrum of SY740 in Fig. 8a at approximately 4.2 ppm is consistent with silanol groups engaged in hydrogen bonding with water with O···O lengths in the range of 2.8 to 3 Å (51). This peak deshields slightly in the 16% w/w dispersion of ezetimibe in SY740, suggesting a stronger hydrogen bonding environment in this material. This environment may involve silanol interactions with ezetimibe, as suggested by the hydrogen bonding effects on the O1 acceptor detected by IR spectroscopy and ^{13}C SSNMR.

The 16% w/w dispersion in SY350 yields a ^{1}H DP-MAS spectrum with a significantly different appearance, with the intensity from the silanol-water peak spread over a greater chemical shift range in comparison to the spectrum of input SY350. The aromatic signals from ezetimibe remain pronounced in the ^{1}H spectrum. The ^{1}H spectrum of this material recorded using the windowed DUMBO sequence, shown in Fig. 8b, again did not offer any improvement in ^{1}H resolution. Minor peaks with highly shielded chemical shifts (<2 ppm) are also observed in the ^{1}H spectra of the input silica materials, particularly in the spectrum of SY350. ^{1}H peaks in this range are commonly associated with isolated silanol groups not engaged in hydrogen bonding (52). These results are also consistent with the weaker hydrogen bonding effects observed for the O1 acceptor in the ezetimibe-SY350 dispersion by IR spectroscopy and ^{13}C SSNMR. The observation of ^{1}H spectra is seen to offer more information about the silanol environment than ^{29}Si CP-MAS or DP-MAS spectra.

Although the ^{1}H spectra of these materials are limited in resolution, even at a field of 16.4 T, the resolution of the spectra is sufficient to distinguish the two components of the mesoporous dispersion, allowing potential correlations to be observed using 2D ^{1}H-^{1}H spin diffusion experiments. This experiment has been used successfully in recent studies of other complex pharmaceutical materials (16,53,54). Spectra were measured using mixing times of 10 μs, 1 ms, 10 ms, 25 ms, 50 ms, 100 ms, and 250 ms, with each 2D spectrum requiring 3 h to obtain. Selected results of 2D ^{1}H-^{1}H spin diffusion experiments performed on the ezetimibe-SY740 dispersion are shown in Fig. 9. The spectra shown in Fig. 9 are representative of the extremes of the series of mixing times, showing the appearance of the 2D spectrum at relatively short (1 ms) and long (100 ms) mixing times. At the 100 ms mixing time, the aromatic proton resonances from ezetimibe in the 6–7 ppm region are observed to correlate strongly with the large silanol-water peak at approximately 4.5 ppm. The spectra thus confirm the presence of an interaction between the drug and the silica. The results

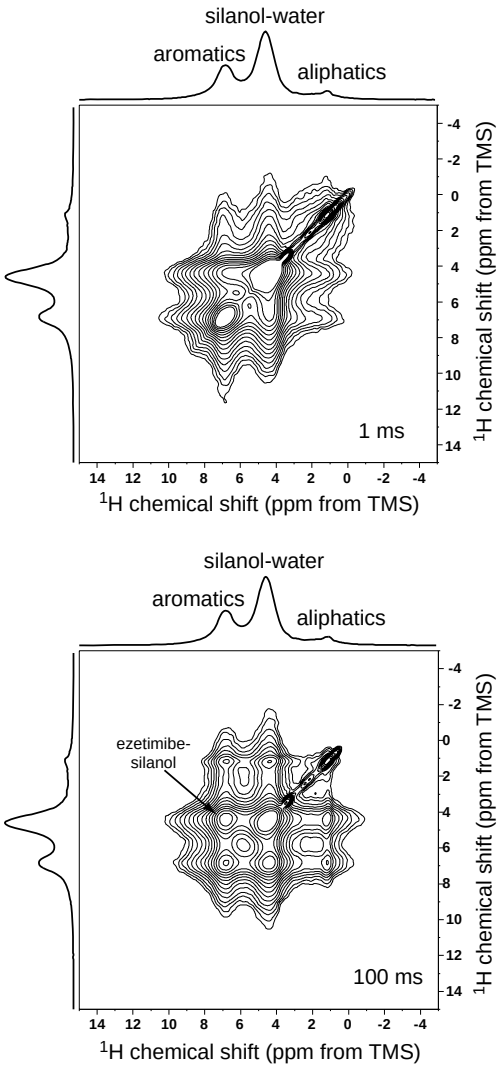

Fig. 9 ^{1}H 2D spin diffusion spectra ($\nu_r = 35$ kHz) of the 16% w/w ezetimibe-SY740 dispersion measured with mixing periods of 1 ms and 100 ms. ^{1}H DP-MAS spectra ($\nu_r = 35$ kHz) are shown plotted along the F_1 (*vertical*) and F_2 (*horizontal*) axes. Spectra were obtained at 16.4 T and 273 K.

of the 2D ^{1}H-^{1}H spin diffusion experiments on the ezetimibe-SY350 dispersion were inconclusive and are not shown. The lack of a clear silanol-water signal in the ^{1}H spectra of the ezetimibe-SY350 dispersion leads to insufficient ^{1}H resolution to detect ezetimibe-silanol correlations, and illustrates a drawback of the 2D ^{1}H-^{1}H spin diffusion approach. A heteronucleus can be employed to avoid this situation at the expense of sensitivity as described below.

2D ^{1}H-^{19}F, ^{1}H-^{13}C, and ^{1}H-^{29}Si CP-HETCOR Experiments

The 2D ^{1}H-^{1}H spin diffusion experiment is limited by the resolution of the ^{1}H spectrum, even at high static magnetic field strengths. The detection of a heteronucleus allows use of lower field strengths that are more widely available at the expense of sensitivity. The ^{1}H dimension of a heteronuclear-detected ^{1}H-X CP-HETCOR experiment can be used to determine whether interactions are occurring between the heteronuclei and the same type of proton environment (14). In the present work, ^{1}H-X CP-HETCOR experiments were performed with X = ^{13}C, ^{19}F, and ^{29}Si to assess these interactions using a modified approach to that presented previously that is better suited to study of a mesoporous silica dispersion (14). An additional 50 ms longitudinal mixing period, wherein the magnetization is stored along the z-axis to allow for extended ^{1}H spin diffusion to occur, was inserted prior to the CP transfer for comparison with experiments performed without this period (16,54). In Fig. 10, the results of these experiments performed with both a standard 2 ms ramp CP period and with the additional 50 ms longitudinal mixing period are shown. Clear correlations are observed involving the intense silanol-water signal at a ^{1}H shift of about 4.5 ppm in the ^{1}H-^{19}F and ^{1}H-^{13}C CP-HETCOR spectra obtained with an additional 50 ms of spin diffusion. The same correlation is also the strongest correlation in the ^{1}H-^{29}Si CP-HETCOR experiment performed in a similar manner. This indicates that ^{1}H environments in both ezetimibe and the silica substrate can engage in spin diffusion to the silanol-water environments, and thus that these two components are associated on the scale of the spin diffusion length, which is in the tens of nm under these conditions (14,16,54).

In Fig. 11, ^{1}H-X CP-HETCOR experiments with X = ^{13}C, ^{19}F, and ^{29}Si are shown for the ezetimibe-SY350 dispersion. The lack of a clear ^{1}H resonance for silanol-water environments in this type of silica makes it more difficult to locate a correlation that can provide connectivity information between the silica and ezetimibe. This issue was seen previously in the 2D ^{1}H-^{1}H spin diffusion spectra of this material, and also affects the spectra in Fig. 11. In spite of the use of a heteronucleus, these experiments do not allow for additional information about association between the two components. However, the spectra do provide additional information that can be linked to structural features. For example, the ^{1}H-^{13}C CP-HETCOR spectrum obtained with 50 ms of spin diffusion shows evidence that aromatic carbon positions in the 110 to 130 ppm region are interacting strongly with more shielded ^{1}H positions. These effects may be intramolecular and/or intermolecular in nature, involving multiple silanol-water sites or possibly other ezetimibe molecules.

^{19}F- and ^{29}Si-Detected ^{1}H T_1 Relaxation Time Measurements

Heteronuclear-detected ^{1}H T_1 experiments are often used to prove phase separation in amorphous systems where the presence of multiple phase-separated components is

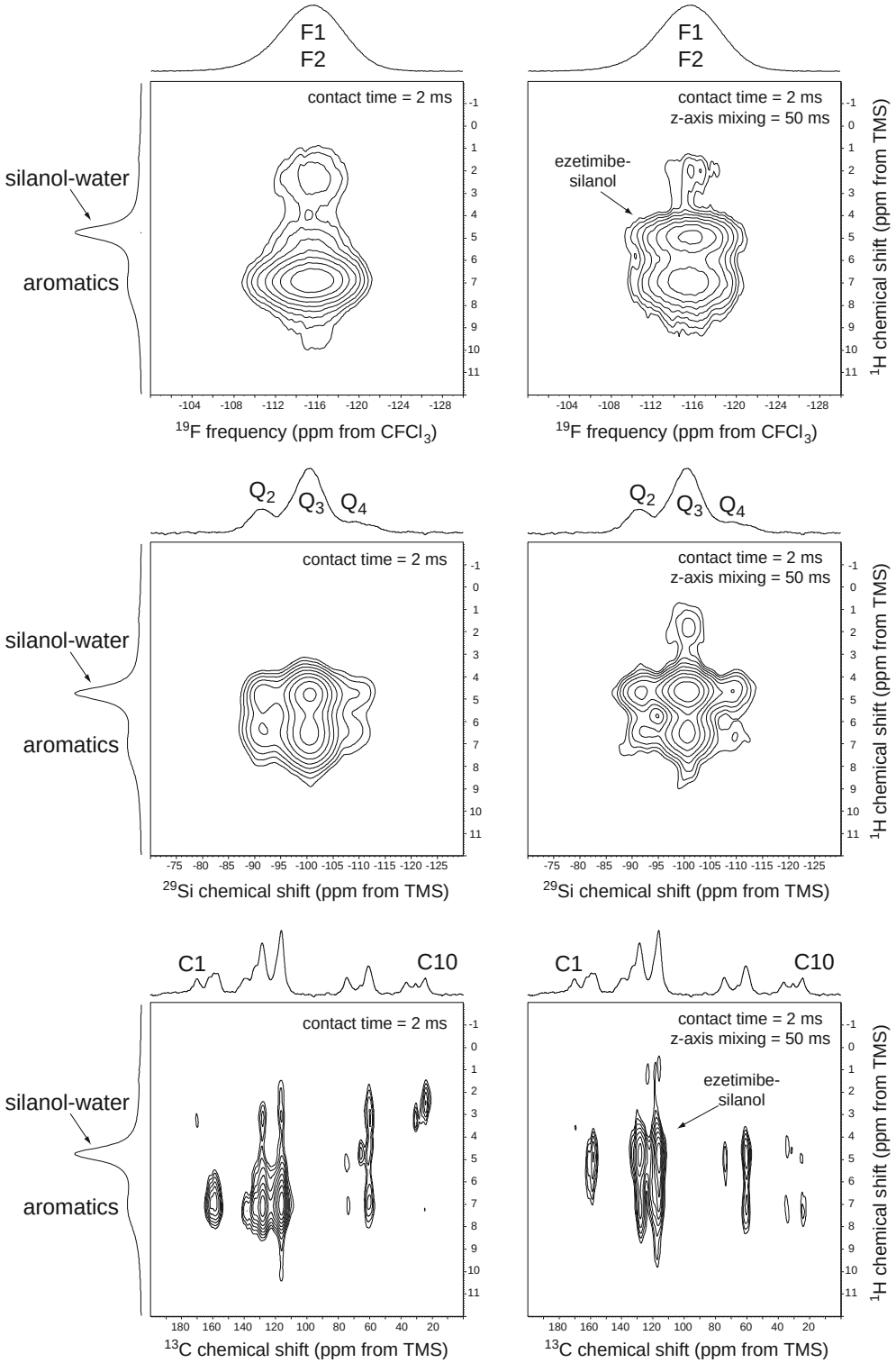

Fig. 10 Comparison of ^{1}H-^{19}F CP-HETCOR (*top*), ^{1}H-^{29}Si CP-HETCOR (*middle*), and ^{1}H-^{13}C CP-HETCOR (*bottom*) spectra of the 16% w/w ezetimibe-SY740 dispersion obtained with 2 ms contact times and with a 50 ms z-axis mixing period. ^{1}H DP-MAS spectra ($\nu_r = 14$ kHz) are shown plotted along the F_1 (*vertical*) axes and CP-MAS spectra (for ^{19}F and ^{29}Si) at $\nu_r = 14$ kHz and ^{13}C CP-TOSS spectra at $\nu_r = 8$ kHz are plotted along the F_2 (*horizontal*) axes. All spectra were obtained at 11.7 T and 273 K.

suspected (14,15). The possibility of using ^{19}F- and ^{29}Si-detected ^{1}H T_1 experiments to detect potential phase separation was also explored in the present work to assess the applicability of these measurements, and to determine if a single homogenous ^{1}H T_1 could be detected in these inherently heterogeneous dispersions. The observation of

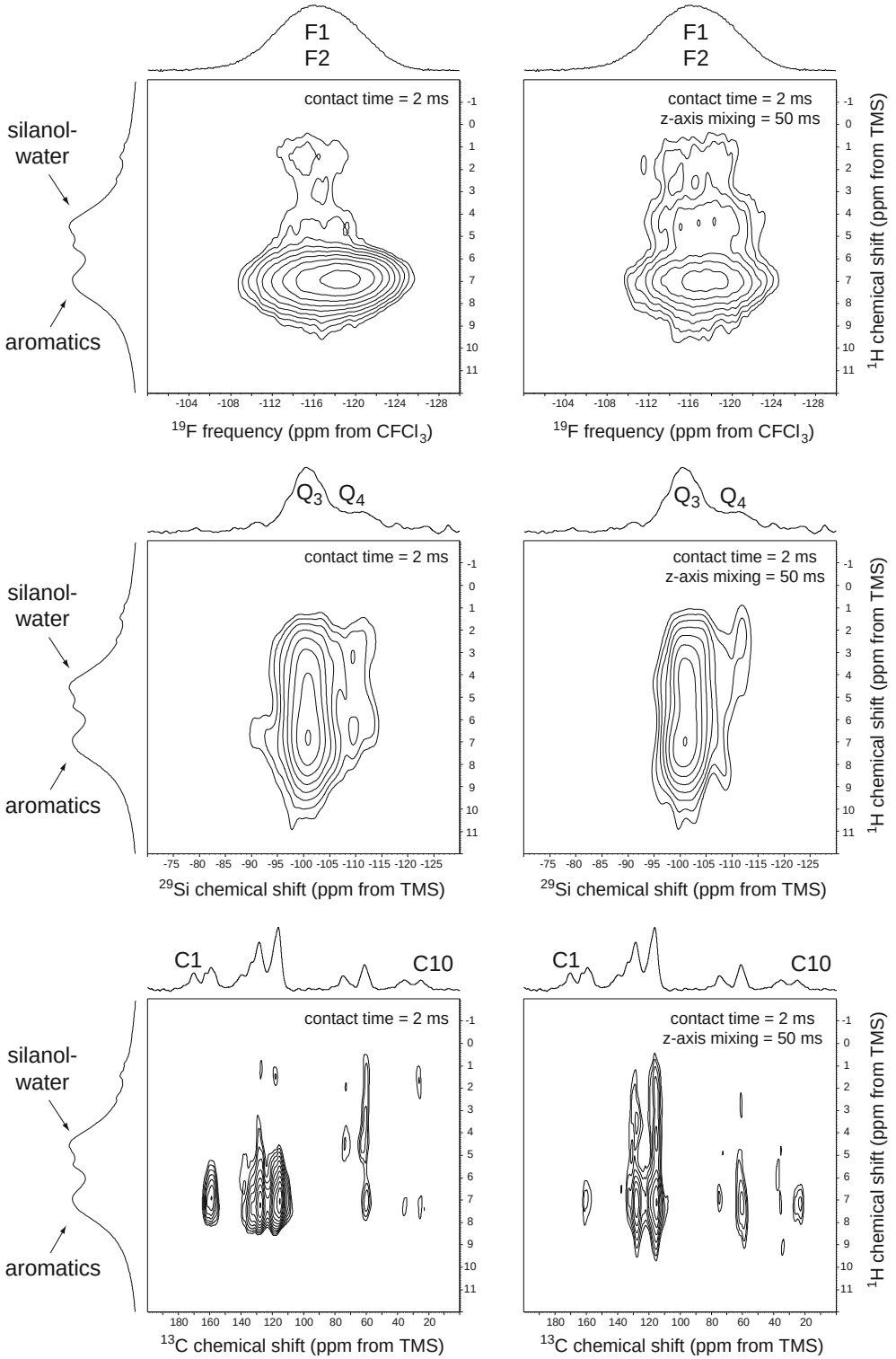

Fig. 11 Comparison of ^{1}H-^{19}F CP-HETCOR (*top*), ^{1}H-^{29}Si CP-HETCOR (*middle*), and ^{1}H-^{13}C CP-HETCOR (*bottom*) spectra of the 16% w/w ezetimibe-SY350 dispersion obtained with 2 ms contact times and with a 50 ms z-axis mixing period. ^{1}H DP-MAS spectra ($\nu_r = 14$ kHz) are shown plotted along the F_1 (*vertical*) axes and CP-MAS spectra (for ^{19}F and ^{29}Si) at $\nu_r = 14$ kHz and ^{13}C CP-TOSS spectra at $\nu_r = 8$ kHz are plotted along the F_2 (*horizontal*) axes. All spectra were obtained at 11.7 T and 273 K.

statistically different ^{19}F- and ^{29}Si-detected ^{1}H T_1 values would imply that the drug-loaded mesoporous materials are sufficiently phase separated as to not allow spin diffusion to equalize relaxation times of protons in silica and in ezetimibe. Unlike previous studies on drug dispersions in organic polymers, the drug and silica components do not

contain a common heteronucleus (such as ^{13}C), which necessitates the comparison of separately-measured ^{19}F-detected and ^{29}Si-detected ^{1}H T_1 values obtained for each component (14,15).

^{1}H T_1 relaxation measurements were performed with $\nu_r = 12.5$ kHz for both the ^{19}F- and ^{29}Si-detected experiments, as the same rate must be used for both sets of experiments to obtain comparable results because of the effects of ν_r on spin diffusion (14). The greater ν_r used for ^{19}F observation was chosen because it provides better resolution for fitting but still allows for sufficient spin diffusion. Five replicate measurements were made for each observed nucleus. For the 16% w/w ezetimibe-SY350 dispersion, the ^{19}F-detected ^{1}H T_1 value was determined to be 0.89 ± 0.14 s and the ^{29}Si-detected ^{1}H T_1 value was found to be 0.86 ± 0.25 s at 298 K and 9.4 T. The greater error in the ^{29}Si-detected result reflects the lower signal-to-noise inherent in each of the time points of the saturation recovery experiment, even using a 12 h acquisition period. The ^{19}F-detected experiments, in comparison, required 3.6 h each. The ^{1}H T_1 values for the SY350 silica and ezetimibe drug are similar and are within the CI of the experiment, as would be expected for a material that behaves as if it is a single phase.

For the 16% w/w ezetimibe-SY740 dispersion, the ^{19}F-detected ^{1}H T_1 value was determined to be 0.69 ± 0.02 s and the ^{29}Si-detected ^{1}H T_1 value was determined to be 0.53 ± 0.09 s at 298 K and 9.4 T. This result was not expected given that association was observed between the components by the 2D experiments and single-phase behavior was thus expected. To assess whether MAS suppression of ^{1}H spin diffusion played a role in the difference observed between these relaxation times, a single replicate was re-measured at a much lower ν_r of 5 kHz (14). The ^{19}F-detected ^{1}H T_1 value was determined to be 0.67 s and the ^{29}Si-detected ^{1}H T_1 value was determined to be 0.53 s, showing no significant change from the results obtained with ν_r set to 12.5 kHz and thus no indication of suppression of spin diffusion by MAS. Single measurements were repeated at 273 K with ν_r set to 5 kHz, and the ^{19}F-detected ^{1}H T_1 value was observed to reduce to 0.50 s and the ^{29}Si-detected ^{1}H T_1 value was found to be 0.38 s. Both T_1 values thus diminish with decreasing temperature, indicating fast motion, which is consistent with the ^{19}F T_1 results reported previously. The potential effect of N_2 ingress from the MAS spinning gas on ^{1}H T_1 values was also considered. In this study, the samples were equilibrated for several days in the MAS rotor (while other spectra were obtained) before ^{1}H T_1 measurements were begun, and the ^{19}F-detected ^{1}H T_1 measurements were performed before and after the ^{29}Si-detected ^{1}H T_1 measurements over a period of 5 days. No trends in the measured relaxation times were observed that could be indicative of additional N_2 ingress during the measurement period for either the ezetimibe-SY740 or ezetimibe-SY350 dispersions. Finally, the ^{1}H spectrum of other types of mesoporous silica in rotors open to the spinning gas is known to be sensitive to N_2 ingress, but no evidence was observed by ^{1}H SSNMR of any substantial changes in the spectra of the present samples after several days of spinning (51). The result is thus unlikely to be an experimental artifact.

Several phenomena could explain the differential ^{1}H T_1 values observed from the 16% w/w ezetimibe-SY740 dispersion. First, this material could be heterogenous on a scale that is too large for ^{1}H T_1 equalization to occur *via* spin diffusion (e.g. tens of nanometers). However, this is not in agreement with the known pore size of the material (2.5 nm) and it is unclear why this effect would not also be observed for the ezetimibe-SY350 dispersion. Alternatively, the differential ^{1}H T_1 results may arise because of the two-fold increase in silica surface area in the ezetimibe-SY740 dispersion and the large number of silanol groups engaged in hydrogen bonding (as observed by ^{1}H SSNMR). Because of this, there may not be enough protons in the bulk of the silica to drive efficient spin diffusion, and ^{1}H T_1 relaxation may occur at solid-gas surfaces more rapidly than spin diffusion into the silica can occur, leading to differential relaxation times. This is supported by the ^{1}H SSNMR spectrum of the ezetimibe-SY350 dispersion, which shows the presence of interior silanol groups not engaged in hydrogen bonding. The differential ^{1}H T_1 results may be related to the ^{19}F T_1 results discussed previously which indicated fast motion in the drug portion of the 16% w/w ezetimibe-SY740 dispersion. The presence of acetone in the ezetimibe-SY740 dispersion, as detected by ^{13}C SSNMR, might act as a plasticizer and further influence the differential ^{1}H T_1 results by increasing mobility in the amorphous drug phase and/or acting as an efficient relaxation sink.

CONCLUSIONS

Amorphous dispersions of ezetimibe adsorbed onto mesoporous silica were characterized using SSNMR and other techniques to determine their structural and dynamical properties and detect interactions between the drug and the silica substrate. ^{19}F CP-MAS experiments were found to be a sensitive method for direct detection of amorphous ezetimibe in these materials. Stronger hydrogen bonding effects between the drug and the silica were observed for the ezetimibe-SY740 dispersion, which was prepared using silica with a larger surface area, through trends observed by IR spectroscopy, ^{1}H spectra of silanol-water environments, and ^{13}C spectra of ezetimibe. Differences in drug mobility were also observed by ^{19}F T_1 and $T_{1\rho}$ experiments, with the ezetimibe-SY740 dispersion exhibiting faster motion in the

MHz frequency range and the ezetimibe-SY350 dispersion showing faster motion in the kHz frequency range.

This study also demonstrated the application of several 2D SSNMR analysis methods to the direct detection of interactions between drug and the mesoporous silica substrate. The 2D SSNMR approach demonstrated here has been applied to silica-supported materials in other fields but has not previously been adapted for pharmaceutical applications. ^{1}H 2D spin diffusion experiments performed at high field provided a sensitive means of detecting interactions between ezetimibe and the silica surface in both the ezetimibe-SY740 and ezetimibe-SY350 dispersions, although the interactions were unclear for the latter dispersion because of limited ^{1}H resolution. The ^{1}H 2D spin diffusion approach is applicable to both fluorinated and non-fluorinated drugs assuming that sufficient ^{1}H resolution can be obtained. Multinuclear 2D HETCOR experiments offered similar results, again showing interactions but also being dependent on the achievable ^{1}H resolution. A 1D ^{19}F-^{29}Si CP experiment, which takes advantage of the presence of fluorine in ezetimibe, was able to directly detect short-range interactions between the ezetimibe and silica in the ezetimibe-SY740 dispersion but not in the ezetimibe-SY350 dispersion.

The set of experiments applied here should be capable of analyzing many mesoporous systems of interest and would also be useful in studies of batch-to-batch variability in pharmaceutical development. The SSNMR methods can be implemented on both low and high-field SSNMR systems using a variety of probe designs. The analyses shown here were accomplished using less than 100 mg of each material of interest, which allows for use of these approaches even when drug supply is limited, such as during early-phase pre-clinical drug development. While a broad set of SSNMR experiments were applied in the present work, it should be noted that other techniques not utilized here, such as sensitivity enhancement *via* the Carr-Purcell-Meiboom-Gill pulse sequence, may be useful in other situations such as in structural studies of mesoporous silica excipients or to enable 2D ^{19}F-^{29}Si CP correlation experiments (55). SSNMR is also highly complementary to other structural techniques, such as neutron vibrational spectroscopy, that have recently been employed in studies of drugs in mesoporous silica (56).

REFERENCES

1. Yu L. Amorphous pharmaceutical solids: preparation, characterization and stabilization. Adv Drug Deliv Rev. 2001;48:27–42.
2. Willart JF, Descamps M. Solid state amorphization of pharmaceuticals. Mol Pharm. 2008;5:905–20.
3. Janssens S, Van den Mooter G. Physical chemistry of solid dispersions. J Pharm Pharmacol. 2009;61:1571–86.
4. Friesen DT, Shanker R, Crew M, Smithey DT, Curatolo WJ, Nightingale JAS. Hydroxypropyl methylcellulose acetate succinate-based spray-dried dispersions: an overview. Mol Pharm. 2008;5:1003–19.
5. Qian KK, Bogner RH. Application of mesoporous silicon dioxide and silicate in oral amorphous drug delivery systems. J Pharm Sci. 2012;101:444–63.
6. Miura H, Kanebako M, Shirai H, Nakao H, Inagi T, Terada K. Influence of particle design on oral absorption of poorly water-soluble drug in a silica particle-supercritical fluid system. Chem Pharm Bull. 2011;59:686–91.
7. Qian KK, Bogner RH. Spontaneous crystalline-to-amorphous phase transformation of organic or medicinal compounds in the presence of porous media. Part 1: thermodynamics of spontaneous amorphization. J Pharm Sci. 2011;100:2801–15.
8. Qian KK, Suib SL, Bogner RH. Spontaneous crystalline-to-amorphous phase transformation of organic or medicinal compounds in the presence of porous media. Part 2: amorphization capacity and mechanisms of interaction. J Pharm Sci. 2011;100:4674–86.
9. Azais T, Tourne-Peteilh C, Aussenac F, Baccile N, Coelho C, Devoisselle JM, *et al.* Solid-state NMR study of ibuprofen confined in MCM-41 material. Chem Mater. 2006;18:6382–90.
10. Azais T, Hartmeyer G, Quignard S, Laurent G, Babonneau F. Solution state NMR techniques applied to solid state samples: characterization of benzoic acid confined in MCM. J Phys Chem C. 2010;114:8884–91.
11. Miura H, Kanebako M, Shirai H, Nakao H, Inagi T, Terada K. Stability of amorphous drug, 2-benzyl-5-(4-chlorophenyl)-6-[4-(methylthio)phenyl]-2H-pyridazin-3-one, in silica mesopores and measurement of its molecular mobility by solid-state ^{13}C NMR spectroscopy. Int J Pharm. 2011;410:61–7.
12. Tanabe S, Higashi K, Umino M, Limwikrant W, Yamamoto K, Moribe K. Yellow coloration phenomena of incorporated indomethacin into folded sheet mesoporous materials. Int J Pharm. 2012;429:38–45.
13. Buntkowsky G, Breitzke H, Adamczyk A, Roelofs F, Emmler T, Gedat E, *et al.* Structural and dynamical properties of guest molecules confined in mesoporous silica materials revealed by NMR. Phys Chem Chem Phys. 2007;9:4843–53.
14. Pham TN, Watson SA, Edwards AJ, Chavda M, Clawson JS, Strohmeier M, *et al.* Analysis of amorphous solid dispersions using 2D solid-state NMR and ^{1}H T_1 relaxation measurements. Mol Pharm. 2010;7:1667–91.
15. Patel JR, Carlton RA, Yuniatine F, Needham TE, Wu L, Vogt FG. Preparation and structural characterization of amorphous spray-dried dispersions of tenoxicam with enhanced dissolution. J Pharm Sci. 2011;101:641–63.
16. Vogt FG, Williams GR. Analysis of a nanocrystalline polymer dispersion of ebselen using solid-state NMR, Raman microscopy, and X-ray diffraction. Pharm Res. 2012;29:1866–81.
17. Khanderia U, Regal RE, Rubenfire M, Boyden T. The ezetimibe controversy: implications for clinical practice. Ther Adv Cardiovasc Dis. 2011;5:199–208.
18. Gulsun T, Gursoy RN, Oner L. Design and characterization of nanocrystal formulations containing ezetimibe. Chem Pharm Bull. 2011;59:41–5.
19. Kiekens F, Eelen S, Verheyden L, Daems T, Martens J, van den Mooter G. Use of ordered mesoporous silica to enhance the oral bioavailability of ezetimibe in dogs. J Pharm Sci. 2012;101:1136–44.
20. Pawley GS. Unit-cell refinement from powder diffraction scans. J Appl Cryst. 1981;14:357–61.
21. Ravikumar K, Sridhar B. Ezetimibe monohydrate. Acta Crystallogr E. 2005;61:o2907–9.

22. McCusker LB, von Dreele RB, Cox DE, Louër D, Scardi P. Rietveld refinement guidelines. J Appl Cryst. 1999;32:36–50.
23. Baldinozzi J, Berar JF. Modeling of line-shape asymmetry in powder diffraction. J Appl Cryst. 1993;26:128–9.
24. Metz G, Wu X, Smith SO. Ramped-amplitude cross-polarization in magic-angle spinning NMR. J Magn Reson A. 1994;110:219–27.
25. Antzutkin ON. Sideband manipulation in magic-angle spinning NMR. Prog Nucl Magn Reson Spectrosc. 1999;35:203–66.
26. Opella SJ, Frey MH. Selection of non-protonated carbon resonances in solid-state NMR. J Am Chem Soc. 1979;101:5854–6.
27. Fung BM, Khitrin AK, Ermolaev K. An improved broadband decoupling sequence for liquid crystals and powders. J Magn Reson. 2000;142:97–101.
28. Hoffner FM, Delmotte L, Kessler H. A $^{19}F/^{29}Si$ CP MAS NMR study of microporous solids synthesized in fluoride medium. Zeolites. 1993;13:60–3.
29. Lesage A, Sakellariou D, Hediger S, Elena B, Charmont P, Steuernagel S, *et al.* Experimental aspects of proton NMR spectroscopy in solids using phase-modulated homonuclear dipolar decoupling. J Magn Reson. 2003;163:105–13.
30. Earl WL, Vanderhart DL. Measurement of ^{13}C chemical shifts in solids. J Magn Reson. 1982;48:35–54.
31. Harris RK, Becker ED, de Menezes SM C, Goodfellow R, Granger P. NMR nomenclature. Nuclear spin properties and conventions for chemical shifts (IUPAC recommendations 2001). Pure Appl Chem. 2001;73:1795–818.
32. Yates JR, Dobbins SE, Pickard CJ, Mauri F, Ghi PY, Harris RK. A combined first principles computational and solid-state NMR study of a molecular crystal: flurbiprofen. Phys Chem Chem Phys. 2005;7:1402–7.
33. Aliev AE, Harris KDM, Apperley DC. High-resolution solid-state ^{13}C and ^{29}Si NMR investigations of the dynamic properties of tetrakis(trimethysilyl)silane. J Chem Soc Chem Commun. 1993; 251–53.
34. Torchia DA. The measurement of proton-enhanced carbon-13 T_1 values by a method which suppresses artifacts. J Magn Reson. 1978;30:613–6.
35. Stejskal EO, Memory JD. High resolution NMR in the solid state. New York: Oxford University Press; 1994. p. 83.
36. van Rossum BJ, Förster H, de Groot HJM. High-field and high-speed CP-MAS ^{13}C NMR heteronuclear dipolar-correlation spectroscopy of solids with frequency-switched Lee-Goldburg homonuclear decoupling. J Magn Reson. 1997;124:516–9.
37. Delley B. An all-electron numerical method for solving the local density functional for polyatomic molecules. J Chem Phys. 1990;92:508–17.
38. Delley B. From molecules to solids with the DMol3 approach. J Chem Phys. 2000;113:7756–64.
39. Boese AD, Handy NC. A new parametrization of exchange-correlation generalized gradient approximation functionals. J Chem Phys. 2001;114:5497–503.
40. Flurchick KM. DFT functionals and molecular geometries. Chem Phys Lett. 2006;421:540–3.
41. Frisch MJ, Trucks GW, Schlegel HB, Scuseria GE, Robb MA, Cheeseman JR, *et al.* Gaussian 09, revision B.01. Wallingford: Gaussian, Inc.; 2010.
42. Becke AD. Density-functional thermochemistry. III. The role of exact exchange. J Chem Phys. 1993;98:5648–52.
43. Chesnut DB, Moore KD. Locally dense basis sets for chemical shift calculations. J Comput Chem. 1989;10:648–59.
44. Bellamy LJ. Advances in infrared group frequencies. New York: Meuthen & Co.; 1968. p. 173–4.
45. Paoloni L, Patta A, Mangano F. The hydrogen bond with carbonyl groups: theoretical study of the correlation between the X-H stretching frequency and the C=O group properties. J Mol Struct. 1975;27:123–37.
46. Mellaerts R, Aerts CA, Humbeeck JV, Augustijns P, Van den Mooter G, Martens JA. Enhanced release of itraconazole from ordered mesoporous SBA-15 silica materials. Chem Commun. 2007;13:1375–7.
47. Kalinowski HO, Berger S, Braun S. Carbon-13 NMR spectroscopy. New York: Wiley; 1987.
48. Stothers JB. Carbon-13 NMR spectroscopy. New York: Academic; 1972. p. 299.
49. Engelhardt G, Michel D. High-resolution solid-state NMR of silicates and zeolites. New York: Wiley; 1987.
50. Bertani P, Raya J, Reinheimer P, Gougeon R, Delmotte L, Hirschinger J. $^{19}F/^{29}Si$ distance determination in fluoride-containing octadecasil by Hartmann-Hahn cross-polarization under fast magic-angle spinning. Solid State Nucl Magn Reson. 1999;13:219–29.
51. Xue X, Kanzaki M. Proton distributions and hydrogen bonding in crystalline and glassy hydrous silicates and related inorganic materials: insights from high-resolution solid-state nuclear magnetic resonance spectroscopy. J Am Ceram Soc. 2009;92:2803–30.
52. Hu JZ, Kwak JH, Herrera JE, Wang Y, Peden CH. Line narrowing in ^{1}H MAS spectrum of mesoporous silica by removing adsorbed H_2O using N_2. Solid State Nucl Magn Reson. 2005;27:200–5.
53. Io T, Fukami T, Yamamoto K, Suzuki T, Xu J, Tomono K, *et al.* Homogeneous nanoparticles to enhance the efficiency of a hydrophobic drug, antihyperlipidemic probucol, characterized by solid-state NMR. Mol Pharm. 2010;7:299–305.
54. Vogt FG, Strohmeier M. 2D solid-state NMR analysis of inclusion in drug-cyclodextrin complexes. Mol Pharm. 2012;9:3357–74.
55. Wiench JW, Lin VSY, Pruski M. ^{29}Si NMR in solid state with CPMG acquisition under MAS. J Magn Reson. 2008;193:233–42.
56. Qian KK, Zhou W, Xu X, Udovic T. Characterization of medicinal compounds confined in porous media by neutron vibrational spectroscopy and first-principles calculations: a case study with ibuprofen. Pharm Res. 2012;29:2432–44.